

9-1999

Stress Distributions in Flowing Aggregated Colloidal Suspensions

Leo Silbert

Southern Illinois University Carbondale, lsilbert@physics.siu.edu

R.S. Farr

J.R. Melrose

R.C. Ball

Follow this and additional works at: http://opensiuc.lib.siu.edu/phys_pubs

○ 1999 American Institute of Physics

Published in [The Journal of Chemical Physics](#), Vol. 111, No.10, September 1999.

Recommended Citation

Silbert, Leo, Farr, R.S., Melrose, J.R. and Ball, R.C. "Stress Distributions in Flowing Aggregated Colloidal Suspensions." (Sep 1999).

This Article is brought to you for free and open access by the Department of Physics at OpenSIUC. It has been accepted for inclusion in Publications by an authorized administrator of OpenSIUC. For more information, please contact opensiuc@lib.siu.edu.

Stress distributions in flowing aggregated colloidal suspensions

L. E. Silbert^{a)}

Advanced Materials Laboratory, Sandia National Laboratories, Albuquerque, New Mexico 87185-1349

R. S. Farr

Unilever Research, Colworth House, Sharnbrook, Bedford, MK44 11Q, United Kingdom

J. R. Melrose

Polymers and Colloids Group, Cavendish Laboratory, University of Cambridge, Madingley Road, Cambridge, CB3 0HE, United Kingdom

R. C. Ball

Department of Physics, University of Warwick, Coventry, CV4 7AL, United Kingdom

(Received 6 November 1998; accepted 16 June 1999)

Simulations of the flow of concentrated aggregated colloidal systems, at the particulate level, are used to investigate the distribution of stresses in the shear-thinning regime. It is found that the distribution of shear stress carried by interparticle bonds decays approximately exponentially at large stresses, but with a double-exponential distribution for values of positive stress. The microstructural mechanisms associated with large stresses are manifested in clusters which dominate the positive contribution to the stress in the system. Towards the end of shear thinning the highest forces occur along bonds defining rods of particles aligned approximately along the flow-compression direction. We propose that the rheology of such systems is determined by a rupture-reformation process of these clusters of stress concentration during the flow. The aggregation forces play the role of enhancing such stress concentration by stabilizing clusters against buckling. © 1999 American Institute of Physics. [S0021-9606(99)51934-X]

I. INTRODUCTION

The flow properties of concentrated and aggregated colloidal suspensions continue to generate great interest not merely because of their relevance to many industrial processes, but also because of the fundamental understanding that is generally lacking in this area. Through the aid of recent numerical and simulation studies, with approximate experimental verification, there now exist many models of the shear behavior of aggregates at low-to-moderate colloid volume fractions, generally, $\phi_c < 0.30$.¹⁻⁵ However, such models make untested assumptions about the evolving dynamics of the microstructure, with many microrheological theories incorporating notions such as the breakup of aggregating bonds in open-particle networks, typically characterized through a fractal-type analysis. The stress is usually considered to exist along chains of particles of strongly aggregated bonds and to be dominated by the extensions of the bonds against the aggregation forces and rupture. Consequently, it has been proposed that aggregating colloidal suspensions necessarily possess a degree of stress concentration, such as along the backbones of such fractal clusters (which are sometimes characterized by the chemical dimension in fractal structures⁶) or at rupture points.

In concentrated systems, we find that the effect of aggregating forces is more subtle. Our model includes the aggregation forces and short-range repulsive springs (these crudely represent polymer coats). We have found that, when

averaged, the dominant contribution to the stress comes from repulsive springs on the particle surfaces—that is, bonds under compression.⁷ Moreover, this contribution is much larger than that of the same system with zero-aggregation force. Yet a perplexing fact is that the direct contribution to the stress from the aggregating forces [c.f. Eq. (3)] is negligible in comparison with the contribution from the surface coats.

Previously,⁷ extensive simulation studies were carried out on the flow behavior of aggregated colloidal suspensions at high colloid volume fractions, $0.47 \leq \phi_c \leq 0.57$. The results borne out in Refs. 7 and 8 yielded many interesting insights regarding the rheology of concentrated, aggregating suspensions—aggregating systems experience a hugely enhanced viscous response over an equivalent nonaggregating system—including semiquantitative agreement with experiment on both the rheology⁹ and also with light-scattering studies.¹⁰

Earlier we computed the shear thinning through to the high shear rate plateau flow regime of our model colloid particles with aggregation forces.⁷ We cannot, with the current code, shear at low enough shear rates to observe the first Newtonian plateau. In the shear-thinning regime, the suspension viscosity η scales with the imposed “simple” shear rate $\dot{\gamma}$ as

$$\eta \sim \dot{\gamma}^{-\alpha}. \quad (1)$$

This power-law, shear-thinning behavior persists over many decades of shear rate. The value of α , the shear-thinning exponent, is found to be independent of ϕ_c in this highly concentrated regime. We note that the value of $\alpha=0.84$ is

^{a)}Electronic mail: lesilbe@sandia.gov

close to values of shear-thinning exponents obtained from experimental studies on concentrated colloids⁹ and “colloidal gels”.^{11,12} In the context of the simulations, the approximately universal relationship, Eq. (1), suggests that the observed power-law, shear-thinning behavior of these concentrated systems is governed by the same mechanisms. Therefore, we do expect a degree of structural evolution generic to the shear-thinning regime, although the concept of open-particle networks is practically unfeasible at these high concentrations.

In our structural analysis of the bulk suspension,⁸ we computed the bulk, steady-state structure factor $S(\mathbf{k})$ over a range of shear rates, both in the shear-thinning regime and beyond. We found that during shear thinning only, $S(\mathbf{k})$ changed very little; liquid-like short-range order exists, plus the presence of a *prepeak* (a correlation peak at lower wave-number k , than that expected for nearest-neighbor correlations—usually situated at approximately integer values of $kd/2\pi$ for particle diameter d). This low- k feature persisted only during shear thinning. The presence of a prepeak in $S(\mathbf{k})$ indicates particle/cluster correlations, suggesting some kind of intermediate range order within the bulk. We also found that this prepeak is not observed in the case of nonaggregating systems. We thus note that in some sense this represents a signature of the observed “universal” shear thinning of aggregated colloids (in the context of our simulations). Ultimately, we wish to gain insight into the structural arrangements of the stress-bearing networks, thus providing a description of what are the mechanisms that control the observed rheology—describing the observed macroscopic behavior through a study of the distribution of forces and stresses between the microstructural constituents.

This approach is motivated by recent studies of dry powders: it may be useful to consider *concentrated* colloidal suspensions as a class of “wet” granular systems. Simply “dry” granular systems (apples packed in a container,¹³ for example) exhibit some rather strange properties which are only recently coming to light.¹⁴ However, we must make the distinction clear that colloidal systems are typically concerned with micron-sized particles with significant thermal agitation as opposed to many real granular systems where particles have dimensions of the order of millimeters if not more. Inertial effects can be neglected in our colloidal simulations, but may play a role in a flowing granular system. Finally, the nature of the dissipative forces differ: colloids in suspension experience viscous hydrodynamic forces, which are dominated by squeeze lubrication modes in concentrated systems; whereas dry granular particles experience shear frictional effects (e.g., Coulombic).

A common finding in studies of two- and three-dimensional granular systems, which has been verified experimentally^{15,16} and by simulation,^{17–19} and also in experimental studies of sheared granular materials,²⁰ is that the distribution of forces (or stresses) in a granular system is extremely inhomogeneous. Such observations have led to the concept of *stress* or *force* chains.^{21–23} A compact granular system under applied stress is typified by a stress distribution which extends out to much larger stresses than the mean—the variance is much larger than the modal value.²⁴ Work at

high packing fractions, on a three-dimensional array of springs, shows that such a strained system exhibits networks of high stress imbedded in a background of a lower-stress-bearing matrix.²⁴ We have previously noted that concentrated colloids under flow exhibit similarly broad distributions.²⁵

The concentration of forces can be used to define networks of contacts, which although only constitute a fraction of the contacts in the system, carry a disproportionate amount of the applied stress. Imaged, these define lines of force or *stress-bearing pathways*. Those “spectator” particles adjoined to this network, but not contributing to the stress propagation, are thus deemed to provide support to the stress-bearing pathways. The directionality of these propagations may be predicted by various methods,^{26,27} and recent progress has been made in describing stress transmission from a statistical mechanical viewpoint.²⁸

We comment that the concepts of stress concentration in granular systems and the fractal-type structures for aggregating colloids at lower ϕ_c are not wholly dissimilar, merely different manifestations of the same problem: stress transmission in a particulate system. It seems that a natural extension of these ideas to the case of flowing colloids may help in the understanding of our concentrated systems. It has already been suggested^{29,30} that certain situations seen in concentrated colloids, such as jammed states, for example,³¹ are better understood in terms of force chains. The similarity between colloidal systems and granular systems are now perceived to be less crude, and indeed, there is currently a large overlap of ideas covering a variety of particulate-based problems. See Ref. 32, for example.

We give a brief description of our model system and the simulation technique employed to study such concentrated systems. To avoid unnecessary repetition, we refer the reader to Refs. 7, 33, and 34 for rather more explicit details. In the results section we investigate the stress distribution problem with a view to elucidating the structures that appear to be controlling the observed flow behavior, and finally, we attempt a qualitative description of the dynamics of these structures through simulation visualization.

II. SIMULATION METHOD

A. Equations of motion

The simulation modeling essentially comprises a version³⁴ of Stokesian dynamics,^{35,36} which enables the study of concentrated colloidal systems by incorporating Lees–Edwards boundary conditions³⁷ on arbitrarily large, defined by the computational box volume Ω , periodic cells. We define the hard-core colloid volume fraction $\phi_c = \pi/6\rho d^3$ of N particles of diameter d , with particle number density $\rho = N/\Omega$. In considering time scales long with respect to the viscous momentum relaxation time of the suspension, we treat the particles at the Langevin/Smoluchowski level and the fluid by the creeping-flow equations. Stick boundary conditions are imposed on the fluid at the particle surfaces.

The equations of motion for N such particles immersed

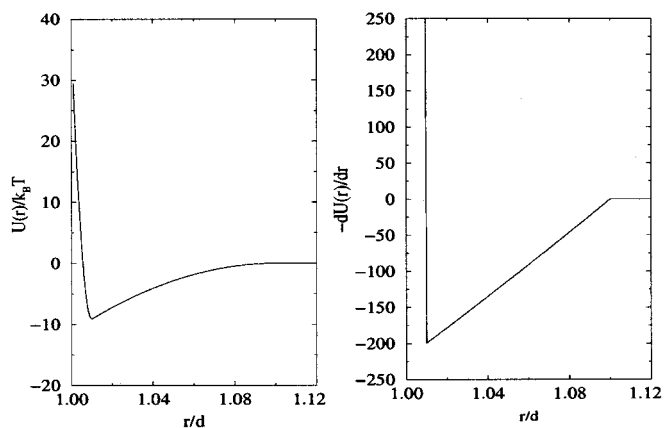


FIG. 1. Interparticle colloid pair-potential $U(r)$, and force law $-dU(r)/dr$, with the following set of parameters; polymer concentration parameter $\phi_p = 0.7$, size ratio $R_g/d = 0.1$, polymer coat thickness $\delta_c = 0.005d$, and $F_0 = 10^4$, giving a maximal attractive force of 200 in these units.

in a Newtonian fluid with viscosity μ thus express a quasi-static force balance:

$$\mathbf{F}^H + \mathbf{F}^P = \mathbf{F}^B = \mathbf{0}. \quad (2)$$

The $6N$ force/torque vectors are: (i) hydrodynamic forces \mathbf{F}^H , exerted on the particles due to their relative motions in the presence of the solvent; (ii) colloidal forces \mathbf{F}^P (the sum of repulsive and attractive terms); and (iii) Brownian forces \mathbf{F}^B .

The terms in \mathbf{F}^H have approximate representations (based on hydrodynamic lubrication theory, see Ref. 38, for example) and their detailed expressions are available elsewhere.^{33,34} The calculation of \mathbf{F}^B is also discussed elsewhere.^{34,39} We refer the reader to Refs. 7, 33, and 34 for discussions on the applicability and general context of the technique used here.

In this work, the colloid forces \mathbf{F}^P are composed of an attractive term, modeled on the Asakura–Oosawa depletion potential—⁴⁰ hence, the term “aggregated” colloids—and a repulsive term, which takes the form of a Hookean spring coat on the surface of the particles; mimicking the osmotic part of an attached/adsorbed polymer layer.

The depletion mechanism assumes a suspension of colloids in a mixture with nonadsorbing polymers of size R_g at volume fraction ϕ_p (which sets the depth of the attractive well). The polymer–colloid size ratio R_g/d , determines the range of the attractive force. The spring coat thickness δ_c sets how much the thermodynamic size of the particle exceeds the hydrodynamic size, and the strength of the spring (which sets the maximal force the spring can supply before collapse) is parametrized by the dimensionless stiffness F_0 . The resulting interaction potential is shown in Fig. 1, and may be thought of as the colloidal equivalent of a Lennard-Jones system. We note here that there exists a maximal attractive force.

The size of the cubic simulation box has side length $L = \Omega^{1/3}$. To provide a reasonable study of structure, here we study systems with $N = 700$, $L \approx 9$. Our ongoing studies for $N = 4000$, in rectangular boxes, give quantitatively identical results. It is only in small systems, say $N \leq 50$, $L \leq 4$, that

system size effects show up in the rheology, for example. We reason that the smallness of the box in small- N simulations interferes with the microstructural mechanisms that give rise to the observed rheology.⁴¹

B. Computation of the stress tensor

In the computation, the bulk stress of the suspension is computed as the sum over nearest-neighbor, interacting particle pairs i and j . We define nearest-neighbor pairs through a neighbor list defined on a three-dimensional tetrahedral Delaunay mesh–Voronoi neighbors. The particle centers on the mesh define the positions of the vertices, and consequently, the mesh edges define particle separations. With this rule, all particles whose centers lie closer than $\sqrt{2}$ (diameters $d = 1$ in the simulation) are neighbors. (We point out that due to this procedure some nearest neighbors will occasionally be slightly beyond the hydrodynamic lubrication approximation range, however, we still employ the approximate hydrodynamic terms regardless.)

The stress is given by

$$\sigma = -\frac{1}{\Omega} \sum_{\alpha} \sum_{ij} \mathbf{f}_{ij}^{\alpha} \mathbf{r}_{ij} + \sigma^B, \quad (3)$$

where the edge vector \mathbf{r}_{ij} is the center–center vector separation from particle i to its neighbor j , and the sum over α is the sum over the various colloid and dissipative forces \mathbf{f}_{ij}^{α} . The Brownian contribution to the stress σ^B is detailed elsewhere.^{34,39} Normalization is with respect to the volume of the computational box Ω .

In steady simple shear, the relation of shear stress to shear rate is conveniently expressed as

$$\sigma_{xy}(\dot{\gamma}) = \mu \eta_r(\dot{\gamma}) \dot{\gamma}, \quad (4)$$

where the xy component of σ represents the shear gradient–flow element of the stress tensor, and μ the solvent viscosity. The measured quantity, the apparent relative viscosity η_r , describes the viscous response due to the imposed shear relative to the base solvent.

This relative viscosity η_r , itself may be decomposed into various contributions arising from the force components where η_r^H and η_r^B denote the hydrodynamic and Brownian contributions to the relative viscosity, and the interparticle colloid force contribution to the viscosity η_r^P , comes from the sum of the repulsive and attractive components.

We measure the imposed shear rate in terms of the accepted nondimensional shear rate the *Peclet* number. In the simulations, the units are chosen so that the particle diameter d , the solvent viscosity μ , and the thermal energy $k_B T$, Boltzmann’s constant times the absolute temperature, are numerically equal to unity. We define the *Peclet* number Pe , as

$$Pe = \frac{\dot{\gamma} d^3 \mu}{k_B T}. \quad (5)$$

In these units, therefore, Pe is the shear rate. Consequently, time is measured in units of $d^3 \mu / k_B T$ and force in units of $k_B T / d$.

Although our simulations do not include Brownian forces, we nevertheless insist on measuring the shear rate in

units of Pe , although it is not strictly correct to do so. Our previous studies³³ on model variations that compares systems with and without Brownian forces show that the inclusion of Brownian forces plays no qualitative role in determining the rheology of such systems.

III. RESULTS

We reiterate some important points from our previous studies.^{7,8,33} Concentrated and aggregated colloids undergo shear thinning over many decades in shear rate, $10^{-4} \leq Pe < 10.0$. In this regime, the viscosity scales with shear rates as in Eq. (1); the suspension microstructure is disordered, liquid-like short-range order exists plus a prepeak. No signs of long-ranged ordering are observed in the shear-thinning regime—ordering is not a feature of shear thinning in concentrated colloids. On average, the dominant contribution (over 90%) to the jump in viscosity between aggregating and nonaggregating systems is the contribution of the repulsive coat interaction.

Beyond the shear-thinning regime, $Pe > 10.0$, the system viscosity levels and the rheology is Newtonian like. Equation (1) no longer applies. The system now possesses a well-ordered structure—the string phase at $\phi_c = 0.50$ (for $Pe > 50.0$) and its rheology is effectively that of hard spheres with repulsive surface coats *without* attractive forces.

A. Stress distributions

To examine the mechanisms that give rise to this rheology, we calculate the distribution of force or stress on bonds in the system under shear. This comprises a histogram of particle pair bonds binned according to the value of the force or stress they carry (we recall that a bond is defined as a Voronoi neighbor). An ensemble, steady-state, average is taken by averaging this over many particle configurations throughout the simulation run.

The viscous response of these systems is characterized by the xy element of the stress tensor—the shear stress (recall $\eta = \sigma_{xy} / \dot{\gamma}$). For convenience we drop the suffix xy when discussing the stress in the system and it should be understood that stress refers to the shear stress.

The stress distribution of a 700-particle system [where the stress is defined as in Eq. (3), i.e., we retain the volume normalization] is plotted in Fig. 2. Here, we focus on one particular shear rate, $Pe = 1.0$ [well into the shear-thinning regime where Eq. (1) holds] at 50% volume fraction. The data in Fig. 2 provide the backdrop to much of the remaining discussion. Variations over shear rate are discussed later.

The different distribution curves in Fig. 2 represent the: total stress (filled circles), squeeze hydrodynamic, Hookean, and the depletion components to the stress. Each of these is computed individually and the normalization of $\omega(\sigma)$ of Fig. 2 is such that the sum over the total number of bonds per configuration N^C is unity, $\sum_{i=1}^{N^C} \omega(\sigma_i) = 1.0$

We note that the two points by the arrow in Fig. 2 indicate that both the total distribution and the squeeze hydrodynamic component distribution go to zero at zero values of the stress. Although the choice of this bin is arbitrary, and we could just as easily avoid this zero bin, we wish to reiterate

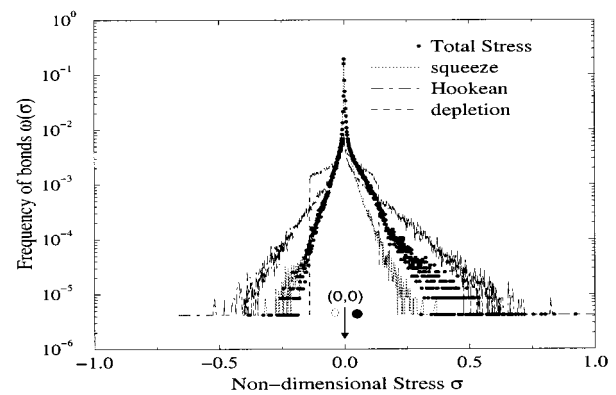


FIG. 2. The stress distribution of the nondimensionalized shear stress per bond for an aggregating system at $\phi_c = 0.50$ being sheared at $Pe = 1.0$. The total and the individual contributions to σ_{xy} are shown. The two points shown by the arrow indicate that both the total and the squeeze curves have points at exactly $(0, 0)$.

an important feature of the simulation technique: there are no bonds which experience zero stress or force. This is to be expected due to the presence of the hydrodynamic forces which couple particle motions over relatively long-ranged distances (compared with the colloid forces). This is a significant feature over those simulations which neglect hydrodynamic interactions and must account for the qualitative differences between the two schemes.

By contrast, the distributions of the colloid forces, the Hookean, and the depletion terms are actually finite at zero stress. A significant fraction of bonds belong to this zero bin, indicating that in the computation of the forces a large fraction of Voronoi neighbor pairs do not interact through the colloid forces, most significantly the Hookean term. Hence, those pairs that do not contribute to the stress must be separated by a distance greater than the interaction range. Even at this high concentration, $\phi_c = 0.50$, this suggests that many of the particles have a separation, $r_{ij}/d > 1.1$. Computation of the average gap does show that on average many of the particle pair bonds are greater than the interaction range.

Several other features are apparent: the total stress distribution extends out to large stresses, with values at least an order of magnitude greater than the peak value. The positive tail of the distribution extends out further than the negative part. The ratio of positive-to-negative stress-carrying bonds is, on average, 67:33. Likewise, the Hookean and the squeeze hydrodynamic stress components to the distribution extend out to large stresses, whereas the depletion term has a finite cutoff to the stress, indicating the maximum force which the depletion term can provide per bond (this was noted in Fig. 1).

From the distribution curve, it is possible to estimate the total stress (and of the components) of the system by averaging over the distribution curve(s),

$$\langle \sigma^{\text{total}} \rangle = \left\langle \sum_{i=1}^{N^C} \omega(\sigma_i) \sigma_i \right\rangle, \quad (6)$$

where an ensemble average, denoted by $\langle \dots \rangle$, is taken over many particle configurations. The average number of particles per configuration N^C provides an estimate of the num-

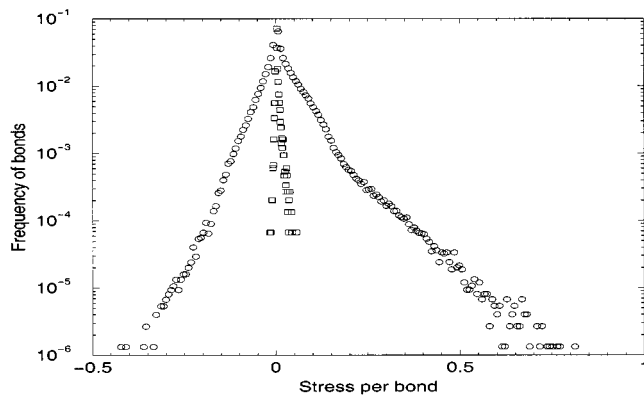


FIG. 3. Comparison of stress distributions for an aggregating system (open circles) and a nonaggregating system (open squares) sheared at $Pe=1.0$.

ber of bonds each particle has attached to it, and hence, an estimation of the average coordination number (the average number of nearest neighbors per particle) N^{nn} . At $Pe=1.0$ and $N=700$, the average number of bonds per configuration sampled over the simulation is computed to be $N^C=5165$. Therefore, the average number of nearest neighbors per particle is $N^{nn}=14$. In the simulations, bonds are defined as Voronoi neighbors. This value of the number of Voronoi neighbors is a little higher than the number of nearest neighbors found in a randomly packed static system of spheres.⁴²

Using these values for N^C and N , the average stress in the system computed using Eq. (6) for the full distribution curve presented in Fig. 2, $\langle\sigma_{dist}\rangle$ is

$$\langle\sigma_{dist}\rangle=43.3,$$

which is to be compared with the computed stress from the simulation rheology data

$$\langle\sigma_{rheo}\rangle=43.2\pm 0.2.$$

Thus, the average stress per bond, assuming that the stress were distributed homogeneously over all the bonds, is $\langle\sigma_{bond}\rangle=8.37\cdot 10^{-3}$.

In studies of granular systems, for example, see Refs. 15, 16, 19, and 20, significant attempts have been made to characterize the distributions in the stresses or forces, a common theme appears to be the exponential decay of the tails at large stresses. Figure 3 shows the distributions of stress per bond on a linear–log plot where we compare the distributions of an aggregating system (circles) with a nonaggregating system (squares), at the same shear rate. We have difficulty in fully characterizing the distribution of the aggregating system, but we reason this is due, in part, to the fact that the aggregating system experiences both compressive and tensile forces, whereas granular systems are mostly concerned with compressive forces only.

Both distributions in Fig. 3 are seen to be dominated by exponential decays. The system without aggregating forces and the bonds with negative stress in the system with aggregating forces are well approximated by a single exponential. However, the bonds carrying positive stress in the system with aggregating forces have a more complex distribution. One identifies three distinct regions. An inner most region (< 0.05) and two outer regions well approximated by expo-

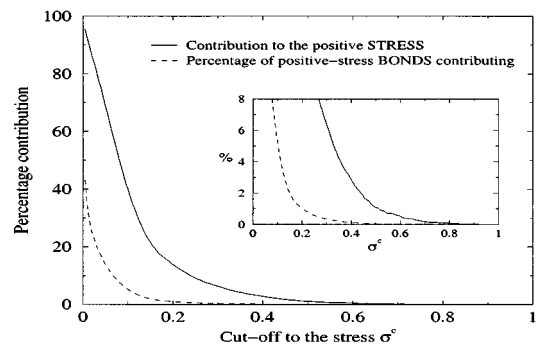


FIG. 4. Percentage contribution to the positive stress coming from positive-stress-carrying bonds and the percentage of those positive-stress-carrying bonds contributing to that amount, for different values of the cutoff σ^c that defines positive-stress-bearing clusters. The inset highlights the low-percentage region.

ponential decays. The second between 0.05 and 0.25 with a slope ~ 10 and the third beyond 0.25 with a slope ~ 20 . There is a slight deviation from exponential in the middle region. The distribution curve kinks around the mean value ~ 0.01 , which roughly coincides with the region where the contribution from the depletion force becomes small relative to the Hookean spring. Study of the distribution curves of the components indicate that the distribution of squeeze stresses also contains a kink in a similar position to that seen in the total distribution curve. The double-exponential form of the distribution curves is also found in simulations of colloid particles at high-shear rates in the regime of shear thickening.⁴³

Also clearly evident in Fig. 3, the aggregating system has a broader distribution than the nonaggregating system, thus reflecting the differences between the macroscopic stress values of each system: the aggregating system has a viscosity almost an order of magnitude greater than the nonaggregating system at this shear rate. Therefore, the generic appearance of exponential decays in stress distributions is more a feature of concentrated particulate systems. Only the quantitative shape of the curves are dependent on the specifics of each system.

The positive side to the distribution must be significant in the determination of the structural mechanisms associated with the distribution of stress, as globally, on the macroscopic scale, the total stress is positive. To investigate this issue the positive part of the stress distribution of the aggregating system is further analyzed in Fig. 4 for a system sheared at $Pe=1.0$.

Figure 4 compares the percentage contribution of the positive stress-carrying bonds to the positive stress when the criterion to be a contributing bond is that the stress it carries is greater than the cutoff value σ^c . The corresponding percentage of stress-carrying bonds contributing at a particular cutoff is also shown. It is clear from the data that a small fraction of positive-stress bonds in the stress computation can actually contribute a significant percentage to the positive stress, justifying the assumed dominance of these high-stress-bearing bonds. For example, bonds which have $\sigma^c > 0.15$ (i.e., over an order of magnitude larger than the av-

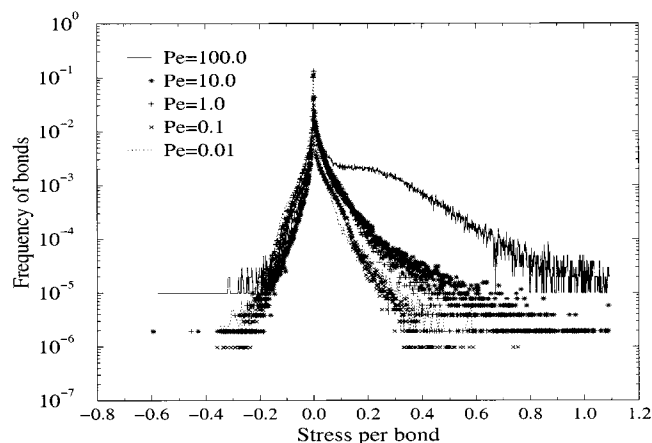


FIG. 5. Stress distributions compared over a range of shear rates: $Pe=0.01$, 0.10 , 1.0 , 10.0 , and 100.0 . The increasing stress with increasing shear rate is seen to be due to the broadening of the positive tail to the distribution.

erage) constitute only 2% of the number of bonds, but 22% of the stress.

B. Variations in shear rate

We analyze the distribution curves over a range of shear rates in Fig. 5. The range of shear rate studied covers the shear-thinning regime, $0.01 \leq Pe < 10.0$, intermediate shear rates $Pe=10.0$, and high shear rates, where ordered phases exist, $Pe=100.0$.

In terms of the distribution curves in Fig. 5, the reason why the stress increases with increasing shear rate is due to the broadening of the positive side of the distributions. The positive bonds are contributing a greater positive stress with increasing shear rate. There is a particular change once the system is at high-shear rates ($Pe=100.0$). The distribution curve at $Pe=100.0$ is qualitatively different from the other curves. A shoulder appears in the distribution up to where the curve is clearly approximately exponential (beyond stress = 0.4). These qualitative differences are mirrored by the rheology where the system at this high-shear rate is no longer shear thinning, and has actually arranged into an ordered flow phase (string phase ordering). We note here that the ordered phase still has an exponential tail, but the high-stress regime is now dominated by the squeeze hydrodynamic contribution rather than the Hookean component which dominated at lower Pe .

IV. STRESS BEARING STRUCTURES

The distribution curves, Fig. 2, show disparities between the stress carried by bonds, but also that many of the bonds are inactive in the sense that they do not contribute to the colloid forces. It is, therefore, hard to see how the high-stress bonds can be evenly distributed throughout the system, and the geometrical arrangements of these bonds should be important. We now investigate the positions of these high-stress bonds within the bulk suspension, and hence, visualize the geometrical arrangements of the structures associated with these bonds. This may be achieved by running a simulation

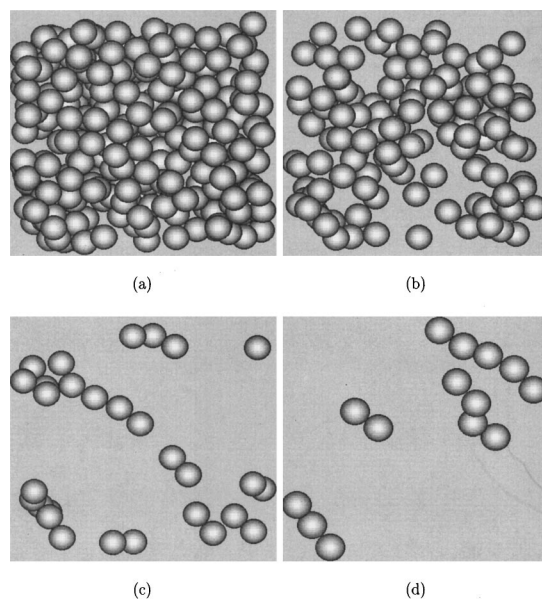


FIG. 6. Clusters of particles whose bonds carry a stress greater than the cutoff value, $\sigma_+^c =$ (a) 0.136, (b) 0.164, (c) 0.204, and (d) 0.250.

and choosing a cutoff to the stress σ_+^c at which to analyze configurations of those particles which belong to these high-stress bonds.

The properties of these dominant bonds are still not clear. This finally brings in the question of structure and kinetics: what *are* the structural mechanisms associated with these bonds and their effect on the remaining particles around them. Figure 6 shows several snapshots of particle clusters which are picked out on the stress that their bonds carry at $Pe=1.0$. The pictures in Fig. 6 show that at the lower stress cutoff, clusters are less well defined as separate entities and exist as multiply connected structures. Even still, although the number of bonds picked out in all the pictures is still only a fraction of the total number of bonds in the system, at lower stress cutoff many of the particles are included in the clusters. However, clearly there is a propensity for the clusters to form elongated structures, leading to rod-like clusters at the higher cutoff.

Figure 7 shows an instantaneous snapshot of a full-size simulation cell, differentiating between the high-stress networks (dark gray), immersed within the bulk suspension (light gray). This picture depicts the arrangement these networks have with respect to the surrounding particles in suspension.

A. Cluster kinetics

Particle clusters, defined on their bond stresses, are forming along the shear-compression direction through which high-stress bonds are continually being formed and broken. However, as yet we do not have a clear idea of their longevity. The snapshots presented in Fig. 6 are instantaneous in time, therefore, they need not represent the absolute configuration of these clusters over longer time periods. The presence of the imposed shear is responsible for the directionality of these clusters—a simple model of shear-induced clustering has been reported⁴⁴ yet intuitively, it is expected

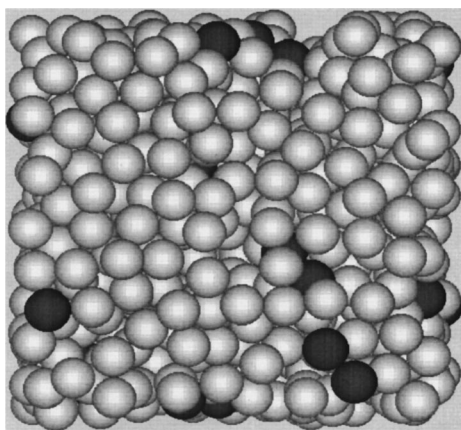


FIG. 7. The whole simulation cell looking into the flow-gradient plane (flow is left to right). The darker particles are picked out on the stress value that their bonds carry. Here, $\sigma_+^c = 0.204$ for $Pe = 1.0$.

that the shear will affect the kinetics of these clusters: the clusters have the possibility to either break, group, or even tumble with the flow. Thus, we need to have some view of the kinetics of these clusters leading to an indication of mechanisms through which these clusters contribute to the stress.

Table I shows how contributions from the high-stress clusters affect the global macroscopic stress. If the fraction of high-stress bonds decreases, the contribution to the stress from these clusters likewise decreases, leading to a lower total (positive) stress. Thus, the chains determine fluctuations in the positive-stress values through their kinetics.

Table I shows how contributions from the high-stress clusters affect the global macroscopic stress. If the fraction of high-stress bonds decreases, the contribution to the stress from these clusters likewise decreases, leading to a lower total (positive) stress. Thus, the chains determine fluctuations in the positive-stress values through their kinetics.

The temporal evolution of these clusters is *qualitatively* examined in Fig. 8. Figure 8 shows a sequence of snapshots of high-stress clusters of particles, separated by, of order, 0.01, 1.0, and 100 units of strain, for a 700-particle system with $\sigma_+^c = 0.204$ at $Pe = 1.0$. Figure 8 presents us with a first view of the kinetics of these clusters. Although the same coloring scheme is used in the each of the four pictures of Fig. 8, the particles composing the clusters viewed in each picture are not necessarily the same as in each of the other pictures of Fig. 8. However, what becomes apparent is the persistence of the geometrical arrangement or orientations of the individual *clusters*. Even though the populations of the clusters are continually changing as the shear flow disrupts the arrangements of individual *particles*, the orientations of these pathways or chains along which the stress propagates persist around the compressional axis (see also Fig. 10).

TABLE I. Comparing the contributions to the total stress from high-stress clusters and the relative number of high-stress bonds in the clusters for different instantaneous values of the stress.

Total positive stress	Fractional contribution from high-stress clusters	Fraction of bonds belonging to these clusters
84.5	0.26	0.020
71.5	0.13	0.009
59.6	0.07	0.005

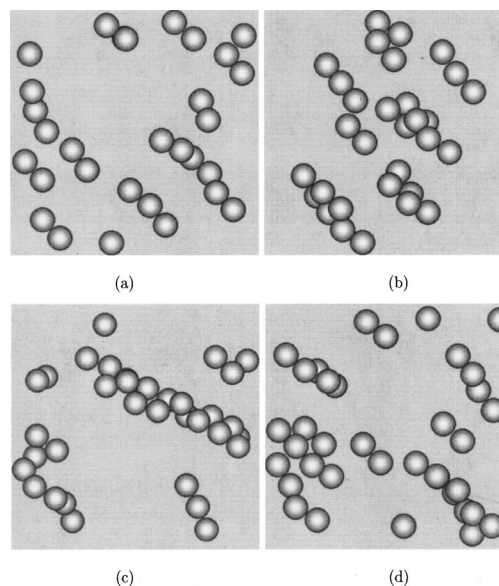


FIG. 8. A qualitative measure of the kinetics of stress bearing clusters at $Pe = 1.0$, for a 700-particle system, where only those particles whose bonds carry a stress greater than $\sigma_+^c = 0.204$, are shown. Strain values are (a) 106.000, (b) 106.013, (c) 107.001, and (d) 289.001.

We plot the distribution of lifetimes of cluster bonds at three different shear rates in Fig. 9. On the linear-log scale we clearly see that these distributions are well characterized by an exponential decay in lifetimes. On average, cluster bonds live for only fractions of a shear time (one shear time \equiv one unit of strain). Thus, it is clear the particles that constitute the stress clusters *are* continually changing and the populations of these clusters evolve with the flow.

The snapshots in Fig. 8 indicate that, at any one instant, the geometrical manifestation of the stress concentration exists as particle clusters that appear as rod-like entities. We have examined this behavior averaged over many configurations—ensemble averaging over long times. Through the simulation scheme we compute the “reduced” structure factor $S^r(\mathbf{k})$, where “*r*” denotes reduced in the sense that these configurations are made up of high-stress clusters only—a subset of the full particle configuration.

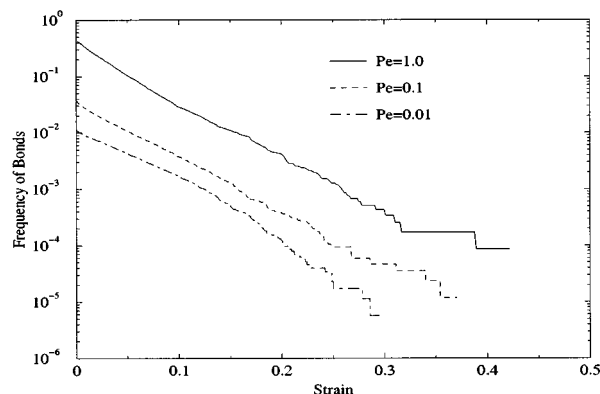


FIG. 9. Distribution of high-stress cluster bond lifetimes at $Pe = 0.01, 0.1,$ and 1.0 (in units of strain γ). Cluster bonds are defined as those bonds experiencing a stress higher than the average bond stress by a factor of ~ 25 .

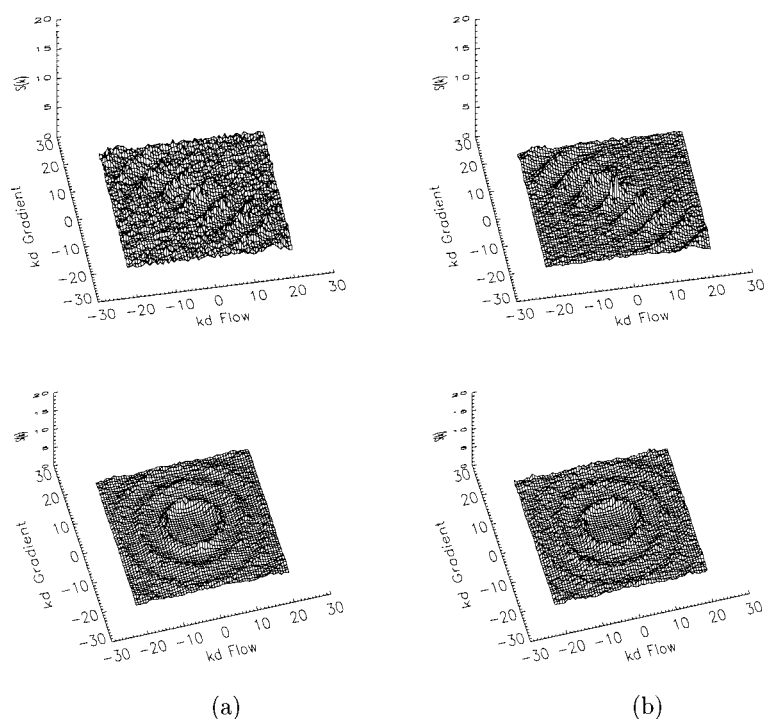


FIG. 10. The “reduced” structure factor $S^r(\mathbf{k})$ (top pictures) computed over many high-stress cluster configurations, compared against the the full $S(\mathbf{k})$ (bottom pictures) for bulk system size $N=700$, sheared at (a) $Pe=0.1$ and (b) $Pe=1.0$. Note the scale of the verticle axis S is different between the top and the bottom pictures.

$S^r(\mathbf{k})$ is computed and we compare these against the corresponding full $S(\mathbf{k})$.

In the $S^r(\mathbf{k})$ (top two pictures of Fig. 10) the regularity of the correlation ridges along the compressional direction are indicative of strong correlations between particles within the same cluster. However, we see that these correlations become less well defined towards lower shear rates, suggesting that with decreasing Pe , the stress-bearing clusters become less rod-like, possibly becoming more multiply connected.

The peaks at low- k suggest correlations over intermediate ranges, between individual clusters. But again, these are diminished at $Pe=0.1$. However, it is suggestive that the emergence of the low- k peaks in the top pictures of Fig. 10, which are due to the stress-bearing clusters, are related to the prepeaks, observed as small bumps at low- k , in total structure factor $S(\mathbf{k})$ (bottom pictures); though the scales are different between $S^r(\mathbf{k})$ and $S(\mathbf{k})$ in Fig. 10.

A further consequence of these high-stress bonds can be inferred from Fig. 11. Because these evolving clusters concentrate the stress, with bonds/chains breaking and reforming over time scales shorter than a shear time, as shown in Fig. 9, one might expect that the short-time viscous response of the system will reflect this behavior. In Fig. 11, the individually sampled viscosities, which are continually averaged to compute the total average viscosity, are shown against strain (time). Over this short-time scale, the sampled viscosity (dotted line) exhibits broad fluctuations about the mean value of the viscosity (solid line).

B. Theoretical discussion

It has been shown that the rheology is controlled by stress concentration into clusters carrying high stress on bonds in compression. The temporal evolution of these

clusters—their kinetics—determines their size and geometrical distribution. Given that there is such a large jump in viscosity on turning on aggregation forces, we need to understand the role of these forces in the concentration of stress. Although the analysis presented here is largely qualitative, it provides an impetus towards a theoretical understanding of these systems. As has been mentioned, current theories on flowing colloids do not seem to be applicable to the concentrated systems studied here. The observation of these extended structures suggests that a many-body treatment is required.

Theories of cluster kinetics have existed since the pioneering works of people like Smoluchowski, etc., for example, see Ref. 6. The many-body, cluster treatment of jamming in Ref. 29 utilizes (Smoluchowski) kinetic equations to explain some of the features observed in simulations of bare hard spheres.^{31,45} The population dynamics, in this case of our stress chains, can be expressed as

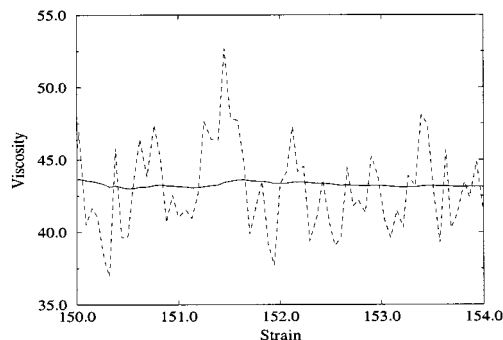


FIG. 11. Variations in the computed viscosity during the simulation. The mean-bulk viscosity is denoted by the solid line, whereas the instantaneously sampled viscosity (dotted line) fluctuates about this mean value.

$$\frac{dn_k}{dt} = \sum_{i,j=1}^{\infty} [K_{ij}n_i n_j - G_{ij}n_{i+j}] (\delta_{i+j,k} - \delta_{i,k} - \delta_{j,k}), \quad (7)$$

where n_k is the concentration of clusters of length kd , d being the particle diameter. However, the real physical problem lies in the ability of correctly interpreting the forms of the aggregation kernel K_{ij} and the breakup kernel G_{ij} , and below we argue the physical mechanisms which these terms describe. A full theoretical treatment, based on an extension of the concepts introduced by Farr, Melrose, and Ball,²⁹ has recently been proposed.⁴⁶

The first term on the right-hand side of Eq. (7) contains information on the rate at which clusters of size i and j produce clusters of size $(i+j)$. Effectively, K accounts for the flow-induced clustering between particles and clusters. The main factor contributing to this term will be the imposed shear rate $\dot{\gamma}$, which sets the time scale for these collisions, as this is the driving force behind particle motions.

If we view the clusters as rods of particles under compression, then the breakup term G is determined by the buckling of these rods. We argue that the role of the aggregation forces is to stabilize the rods against buckling—thereby setting a time scale for the lifetime of these rods—and hence, enhancing the compression of the springs within the rods. To buckle, the rods must break aggregation forces on neighboring spectator particles. It is through this mechanism that the aggregating forces enhance the shear stress despite their negligible contribution on average.

The time scale of breakup will have a dispersion depending on the local motions of the particles. This may then account for the slight variations in the shear-thinning behavior between model variations studied previously.³³

There has been considerable work on describing the rheology of aggregated suspensions in terms of cluster kinetics. Such works attempt to include the relevance of the attractive forces in determining the escape times of particles from bonded chains within fractal aggregates⁴ and in more concentrated systems.⁴⁷ Coarser-grained models also exist⁴⁸ following energy landscape arguments, offering an alternative view.

V. SUMMARY

Flow simulations that include an approximate form for the hydrodynamic interactions in concentrated systems show that the distribution of stresses in flowing aggregated suspensions exhibit similarities with stress distributions in granular systems, characterized by an approximately exponential decay at large stresses, whereby a fraction of bonds experience a stress one to two orders of magnitude larger than the mean value.

The large stresses appear to be localized in only a small fraction of the total number of bonds between particles, giving rise to particle clusters defined on the high stress that they carry. These clusters appear to dominate the positive contribution to the stress, and hence, the macroscopic behavior. Essentially, we define a form of inhomogeneity according to some criterion, in this case, particle structures based on stress. However, we note with caution that we have only

considered one of the aspects of “microstructural inhomogeneities.” Anisotropy in the directionality of the forces *or* the anisotropy in the particle contacts are both likely,⁴⁹ but which of these dominates in each regime is still not clear. We hope to report on such studies in the future. The discrete regions of this stress concentration are necessarily generated by the imposed shear with evolving populations of particles, where cluster bond lifetimes are typically less than a shear time.

The stress may also be computed from a dissipation argument, whereby the disturbance that the clusters cause on the surrounding fluid causes an equivalent viscous response through mean-field fluid power dissipation. Whether the greatest dissipation occurs around the clusters, or within the cluster bonds themselves, has not yet been resolved, and we have not yet been able to reconcile such a mechanism with the effects studied here. We hope to answer these questions in the near future.

It is proposed that the kinetics of the stress chains can be described by a Smoluchowski-type kinetic equation. By taking into consideration the rate at which shear-induced clustering occurs, and the rate at which particle bonds are broken (which is highly dependent on the strength of the attractive forces), this theory⁵⁰ provides a first attempt at a many-body approach to flowing colloids.

ACKNOWLEDGMENTS

This research was supported by the external Unilever Colloid Physics Program and the BBSRC food directorate, together with Dalgety plc., and the EPSRC under Grant No. GR/L21747. The authors would like to thank K. G. Soga for many useful discussions.

¹R. Wessel and R. C. Ball, Phys. Rev. A **46**, R3008 (1992).

²A. H. L. West, J. R. Melrose, and R. C. Ball, Phys. Rev. E **49**, 4237 (1994).

³V. Chaplain, P. Mills, and M. Djabourov, Colloid Polym. Sci. **272**, 991 (1994).

⁴A. A. Potanin, R. de Rooij, D. van den Ende, and J. Mellema, J. Chem. Phys. **14**, 5845 (1995), and references therein.

⁵A. A. Potanin and W. B. Russel, Phys. Rev. E **53**, 3702 (1996).

⁶R. Jullien and R. Botet, *Aggregation and Fractal Aggregates* (World Scientific, Singapore, 1987).

⁷L. E. Silbert, J. R. Melrose, and R. C. Ball, J. Rheol. **43**, 673 (1999).

⁸L. E. Silbert, J. R. Melrose, and R. C. Ball, Mol. Phys. **96**, 1667 (1999).

⁹R. Buscall, J. I. McGowan, and A. J. Morton-Jones, J. Rheol. **37**, 621 (1993).

¹⁰H. Verduin, B. J. de Gans, and J. K. G. Dhont, Langmuir **12**, 2947 (1996).

¹¹S. Jogun and C. F. Zukoski, J. Rheol. **40**, 1211 (1996).

¹²H. Huang and C. M. Sorensen, Phys. Rev. E **53**, 5075 (1996).

¹³J. Grindlay, Am. J. Phys. **61**, 469 (1993).

¹⁴*Granular Matter An Interdisciplinary Approach*, edited by A. Mehta (Springer, New York, 1994).

¹⁵C. h. Liu, S. R. Nagel, D. A. Schecter, S. N. Coppersmith, S. Majumdar, O. Narayan, and T. A. Witten, Science **269**, 513 (1995), and references therein.

¹⁶D. M. Mueth, H. M. Jaeger, and S. R. Nagel, Phys. Rev. E **57**, 3164 (1998).

¹⁷S. N. Coppersmith, C. h. Liu, S. Majumdar, O. Narayan, and T. A. Witten, Phys. Rev. E **53**, 4673 (1996), and references therein.

¹⁸M. Nicodemi, Phys. Rev. Lett. **80**, 1340 (1998), and references therein.

¹⁹F. Radjai, M. Jean, J.-J. Moreau, and S. Roux, Phys. Rev. Lett. **77**, 274 (1996), and references therein.

²⁰B. Miller, C. O'Hern, and R. P. Behringer, Phys. Rev. Lett. **77**, 3110 (1996), and references therein.

- ²¹S. F. Edwards and C. C. Mounfield, *Physica A* **226**, 1 (1996).
- ²²M. E. Cates, J. P. Wittmer, J.-P. Bouchaud, and P. Claudin, *Phys. Rev. Lett.* **81**, 1841 (1998).
- ²³C. Thornton, *Kona Powder Particle* **15**, 81 (1997).
- ²⁴A. Pavlovitch, *J. Phys. I* **7**, 1 (1997).
- ²⁵J. R. Melrose, J. H. van Vliet, L. E. Silbert, R. C. Ball, and R. Farr, in *Modern Aspects of Colloidal Dispersions*, edited by R. H. Ottewill and A. R. Rennie (Kluwer Academic, Dordrecht, 1998), p. 133.
- ²⁶P. Claudin, J.-P. Bouchaud, M. E. Cates, and J. P. Wittmer, *Phys. Rev. E* **57**, 4441 (1998).
- ²⁷V. M. Kenkre, J. E. Scott, E. A. Pease, and A. J. Hurd, *Phys. Rev. E* **57**, 5841 (1998).
- ²⁸S. F. Edwards and D. V. Grinev, *Physica A* **263**, 545 (1999).
- ²⁹R. S. Farr, J. R. Melrose, and R. C. Ball, *Phys. Rev. E* **55**, 7203 (1997).
- ³⁰M. E. Cates, J. P. Wittmer, J.-P. Bouchaud, and P. Claudin, *Physica A* **263**, 354 (1999).
- ³¹J. R. Melrose and R. C. Ball, *Europhys. Lett.* **32**, 535 (1995).
- ³²S. F. Edwards and D. V. Grinev, cond-mat/9905114 (submitted to *Jamming and Rheology*, edited by A. Liu and S. R. Nagel (Francis Taylor, New York, 1999) (unpublished).
- ³³L. E. Silbert, J. R. Melrose, and R. C. Ball, *Phys. Rev. E* **56**, 7067 (1997).
- ³⁴R. C. Ball and J. R. Melrose, *Physica A* **247**, 444 (1997).
- ³⁵G. Bossis and J. F. Brady, *J. Chem. Phys.* **80**, 5141 (1984).
- ³⁶L. Durlafsky, J. F. Brady, and G. Bossis, *J. Fluid Mech.* **180**, 21 (1987).
- ³⁷A. W. Lees and S. F. Edwards, *J. Phys. C* **5**, 1921 (1972).
- ³⁸S. Kim and S. J. Karrila, *Microhydrodynamics: Principles and Selected Applications, Series in Chemical Engineering* (Butterworth-Heinemann, Washington, DC, 1991).
- ³⁹G. Bossis and J. F. Brady, *J. Chem. Phys.* **91**, 1866 (1989).
- ⁴⁰W. B. Russel, D. A. Saville, and W. R. Schowalter, *Colloidal Dispersions* (Cambridge University, Cambridge, 1991).
- ⁴¹L. E. Silbert, Ph.D. thesis, University of Cambridge (1998).
- ⁴²J. D. Bernal and J. Mason, *Nature (London)* **185**, 68 (1960).
- ⁴³J. R. Melrose (unpublished).
- ⁴⁴O. J. O'Loan, M. R. Evans, and M. E. Cates, *Physica A* **258**, 109 (1998).
- ⁴⁵R. C. Ball and J. R. Melrose, *Adv. Colloid Interface Sci.* **59**, 19 (1995).
- ⁴⁶R. S. Farr, L. E. Silbert, R. C. Ball, and J. R. Melrose (unpublished).
- ⁴⁷Y. Baxter-Drayton and J. F. Brady, *J. Rheol.* **40**, 1027 (1997).
- ⁴⁸P. Sollich, *Phys. Rev. E* **58**, 738 (1998).
- ⁴⁹F. Radjai, D. E. Wolf, M. Jean, and J.-J. Moreau, *Phys. Rev. Lett.* **80**, 61 (1998), and references therein.
- ⁵⁰R. S. Farr, Ph.D. thesis, University of Cambridge (1998).